blood®
Regular Article

LYMPHOID NEOPLASIA

Endothelial cell–leukemia interactions remodel drug responses, uncovering T-ALL vulnerabilities

Luca Vincenzo Cappelli,[1,2,*] Danilo Fiore,[1,3,4,*] Jude M. Phillip,[5,*] Liron Yoffe,[1,6,*] Filomena Di Giacomo,[1,*] William Chiu,[1] Yang Hu,[6] Clarisse Kayembe,[1] Michael Ginsberg,[7] Lorena Consolino,[8] Jose Gabriel Barcia Duran,[9] Nahuel Zamponi,[10] Ari M. Melnick,[10] Francesco Boccalatte,[11] Wayne Tam,[1] Olivier Elemento,[6] Sabina Chiaretti,[2] Anna Guarini,[2] Robin Foà,[2] Leandro Cerchietti,[10] Shahin Rafii,[9] and Giorgio Inghirami[1]

[1]Department of Pathology and Laboratory Medicine, Weill Cornell Medicine, New York, NY; [2]Department of Translational and Precision Medicine, Sapienza University of Rome, Rome, Italy; [3]Department of Molecular Medicine and Medical Biotechnology, University of Naples Federico II, Naples, Italy; [4]Institute for Experimental Endocrinology and Oncology "G. Salvatore" (IEOS), National Research Council (CNR), Naples, Italy; [5]Departments of Biomedical Engineering, Chemical and Biomolecular Engineering, Oncology, Institute for Nanobiotechnology, Johns Hopkins University, Baltimore, MD; [6]Institute for Computational Biomedicine and Caryl and Israel Englander Institute for Precision Medicine, Weill Cornell Medicine, New York, NY; [7]Angiocrine Bioscience, San Diego, CA; [8]Department of Molecular Biotechnology and Health Sciences, University of Turin, Turin, Italy; [9]Ansary Stem Cell Institute, Division of Regenerative Medicine, Department of Medicine, Weill Cornell Medicine, New York, NY; [10]Hematology and Oncology Division, Department of Medicine, Weill Cornell Medicine and the New York Presbyterian Hospital, New York, NY; and [11]Department of Pathology, New York University School of Medicine, New York, NY

KEY POINTS

- We identified active compounds in a library of 22 T-ALL PDX and discovered public and private vulnerabilities
- Interacting ECs and T-ALL underwent reciprocal transcriptomic changes

T-cell acute lymphoblastic leukemia (T-ALL) is an aggressive and often incurable disease. To uncover therapeutic vulnerabilities, we first developed T-ALL patient–derived tumor xenografts (PDXs) and exposed PDX cells to a library of 433 clinical-stage compounds in vitro. We identified 39 broadly active drugs with antileukemia activity. Because endothelial cells (ECs) can alter drug responses in T-ALL, we developed an EC/T-ALL coculture system. We found that ECs provide protumorigenic signals and mitigate drug responses in T-ALL PDXs. Whereas ECs broadly rescued several compounds in most models, for some drugs the rescue was restricted to individual PDXs, suggesting unique crosstalk interactions and/or intrinsic tumor features. Mechanistically, cocultured T-ALL cells and ECs underwent bidirectional transcriptomic changes at the single-cell level, highlighting distinct "education signatures." These changes were linked to bidirectional regulation of multiple pathways in T-ALL cells as well as in ECs. Remarkably, in vitro EC-educated T-ALL cells transcriptionally mirrored ex vivo splenic T-ALL at single-cell resolution. Last, 5 effective drugs from the 2 drug screenings were tested in vivo and shown to effectively delay tumor growth and dissemination thus prolonging overall survival. In sum, we developed a T-ALL/EC platform that elucidated leukemia-microenvironment interactions and identified effective compounds and therapeutic vulnerabilities.

Introduction

T-cell acute lymphoblastic leukemia/lymphoma (T-ALL/LBL)[1] is an aggressive hematological malignancy with high treatment failure and poor overall survival (OS).[2-4] Developments in therapy and stem cell transplants have improved the event-free survival rates of young patients (~80%). However, refractory/relapsed pediatric (~20%) and adult patients with T-ALL (~40%) often die of the disease.[5,6]

The original stratification of T-ALL (European Group for the Immunological Classification of Leukemia [EGIL] scoring system) highlights a class of early T-cell precursor acute lymphoblastic leukemia: ETP-ALL, representing ~5% to 15% of T-ALL. Patients with ETP-ALL have significantly worse survival,[7,8] a course improved via intensive asparaginase-based regimens.[5] Within T-ALL, the deregulated expression of multiple transcription factors and CDKN2A/2B cell-cycle regulators, and hyperactive NOTCH1 signaling, were initially described as key genomic aberrations. Furthermore, defects affecting Janus kinase/signal transducer and activator of transcription (JAK/STAT) signaling, protein translation, and epigenetic control provide novel and attractive targets for therapy.[9-13] Of note, the implementation of transcriptional signatures is providing actionable diagnostic criteria and improved clinical management.[14]

The cancer microenvironment plays a critical role[15-17] in modulating cell growth and therapeutic responses.[16-19] Within the T-ALL niche, collective protumorigenic signals arise from multiple cellular and noncellular components. Notably, tumor-associated endothelial cells (TECs) are crucial in the pathogenesis of solid and liquid malignancies,[20-22] ultimately

contributing to multiple protumorigenic phenotypes. In T-ALL, TECs modulate leukemic extravasation[23] and tumor aggressiveness via multiple and synergistic mechanisms, including SDF1α/CXCR4, DLL4-JAG1-2/NOTCH, and IGFBP7/IGF1 prosurvival pathways.[18,24,25] However, it is unclear how these individual compartments contribute to the education of leukemic and microenvironment cells. Importantly, the microenvironment can affect drug responses[15,26] via dysregulated chemokine signals,[27] enhanced production of oxidative radicals and exosomes,[28] and hypoxia.[29] As a result, therapies targeting microenvironment cells are predicted to improve clinical responses.[30,31] However, the influence of endothelial-based cultures on perturbing drug responses has not been fully explored yet.

By taking advantage of endothelial cells (ECs) transduced with E4ORF1 (E4-ECs),[32,33] we developed an endothelial-leukemia platform to explore the subverted role of tumor vascular niches. This platform integrates T-ALL patient–derived tumor xenografts (PDXs) and ECs with drug-screening libraries, ultimately translating findings to in vivo preclinical trials. This approach led to the generation of proof-of-concept transcriptional signatures that are predictive of drug response, and the selection of effective compounds/combinations in T-ALL. More importantly, we show that T-ALL and ECs bidirectionally modulate their transcriptomes and phenotypes, and ECs provide signals counteracting the efficacy of selected drugs.

We established an EC-based platform to unveil new microenvironment-leukemia interactions and cancer vulnerabilities. We anticipate that this approach could foster the design of precision medicine–based approaches to improve the treatment of patients with T-ALL.

Methods

Patient material

Pathological samples from bone marrow or peripheral blood (blasts, >80%) were collected at the Hematology Center of Sapienza University of Rome or Weill Cornell Medicine of New York. Diagnoses were assigned based on the World Health Organization classification. According to the Declaration of Helsinki, deidentified patient samples were obtained with informed consent. The institutional review boards of Sapienza University of Rome and Weill Cornell Medicine approved human studies.

PDX generation

PDX implantation and propagation were previously reported.[34] Briefly, fresh or cryopreserved patient samples were implanted into NOD.Cg-*B2m*^{tm1Unc} *Prkdc*^{scid} *Il2rg*^{tm1Wjl}/SzJ (NSG B2m) mice. Animals were euthanized when lymphoblastic cells represented at least 50% of the total circulating blood cells. Serial passages were achieved by IV injection into NOD.Cg-*Prkdc*^{scid} *Il2rg*^{tm1Wjl}/SzJ (NSG) mice. Animal studies were approved by the Weill Cornell Medicine Animal Care and Use Committee (2014-0024).

Flow cytometry

Flow cytometry was performed as described previously,[35] using dedicated instrumentations (BD LSR II, BD FACSCanto flow cytometers and BD FACSCelesta with plate reader for high-throughput screenings) and high-speed sorting (BD Aria).

Cell culture, stimulating factors, and drug screening

PDX-derived T-ALL cells were cultured in RPMI with 10% fetal calf serum (FCS) or StemSpan (SS; StemCell Technologies) supplemented with 10% knockout serum replacement (KSR; Life Technologies) and a cocktail of antibiotics and interleukins (see supplemental Data, available on the *Blood* website). Human umbilical vein endothelial cells transduced with a lentiviral gene transfer vector expressing the *E4-ORF1* gene (VeraVec ECs; Angiocrine Bioscience), namely E4-ECs. Monolayers of E4-ECs were cultured in ex vivo medium supplemented with 10% FCS (Lonza) and maintained at 37°C in a humidified 5% CO_2 atmosphere. Compounds for the drug screenings were purchased from Selleckchem and tested for 72 hours (at least in duplicate) at a concentration of 1.0 μM or in dose-response dilutions where specified. The 433-drug screenings were executed in 384-well plates under either RPMI (plus 10% FCS) or SS (plus 10% KSR) conditions, and the viability was assessed using the CellTiter-Glo assay (Promega). The EC/T-ALL coculture screenings were performed in 96-well plates, and data were collected using the high-throughput screening flow cytometer. The gating strategy was based on appropriately compensated settings for multicolor flow cytometry (propidium iodide for cell death, CFSE for EC labeling, and cell tracer violet for T-ALL cells). To provide uniform measures of drug effects and to estimate EC rescue, we computed specific cell death by normalizing viability on drug exposure with the viability of matched DMSO controls [formula: (death under drug x) – (death of control)/(100 – death of control) × 100]. Drugs were defined as active when able to kill more than 50% of leukemic cells compared with controls.

Total RNA and single-cell RNA sequencing

Refer to the supplemental Methods for details.

In vivo treatment

Mice underwent IV injection (1 × 10^6 T-ALL cells), and engraftment was assessed by flow cytometric analysis of peripheral blood cells. When human T cells reached 5% of the total, mice were randomized into untreated (vehicle) and treated arms. Numbers, age, and sex of the mice were equally distributed among arms. Compounds were administered as described in the figure legends and in the supplemental Methods. Tumor burden was monitored by flow cytometric analysis of peripheral blood or spleen size, using total body magnetic resonance imaging (MRI) or measurements post-autopsy. Body weight was used as a surrogate for drug toxicity.

Statistics

The appropriate statistical methods were applied as indicated in the related figure legends. Continuous variables were analyzed on the basis of normal distribution and homogeneity of variance. The Kaplan-Meier method and log-rank test were used to assess survival.

Tests were performed with Prism version 9.0 (GraphPad, San Diego, CA), MATLAB version 9.0 (MathWorks, Natick, MA),

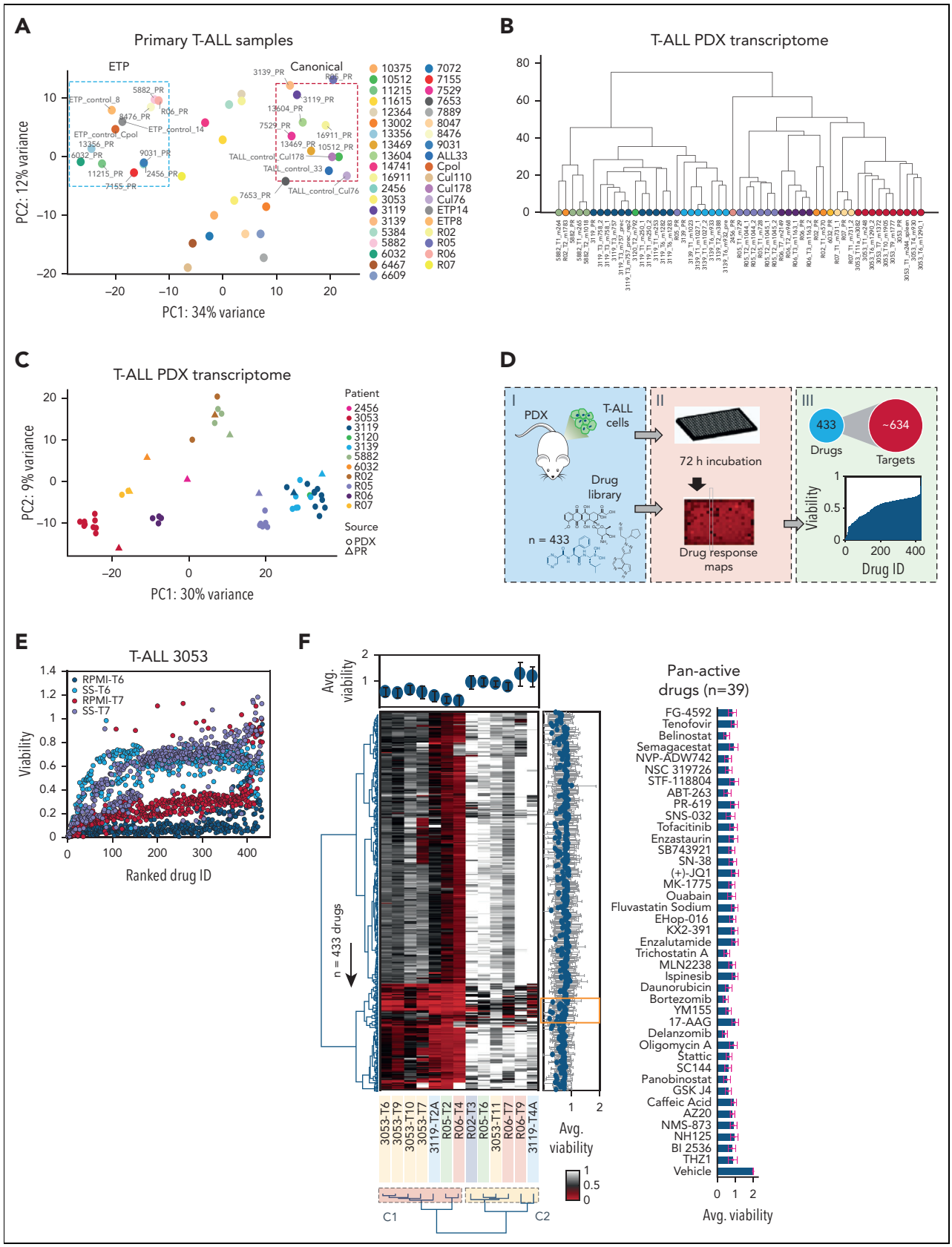

Figure 1. High-throughput screening of T-ALL patient–derived tumor xenografts (PDXs) defines therapeutic responses ex vivo. (A) Principal component analysis of 39 T-ALL primary samples separated into 2 major subgroups corresponding to ETP and canonical T-ALL. A third group with an intermediate phenotype could also be identified. (B) Unsupervised hierarchical clustering of RNA expression profiles among 10 T-ALL PDXs sequenced over multiple passages, including primary (PR) and serial (T) samples. (C) Principal component analysis of 10 T-ALL PDXs sequenced over multiple passages, including PR and serial passages. (D) Scheme illustrating the drug screening of T-ALL PDXs

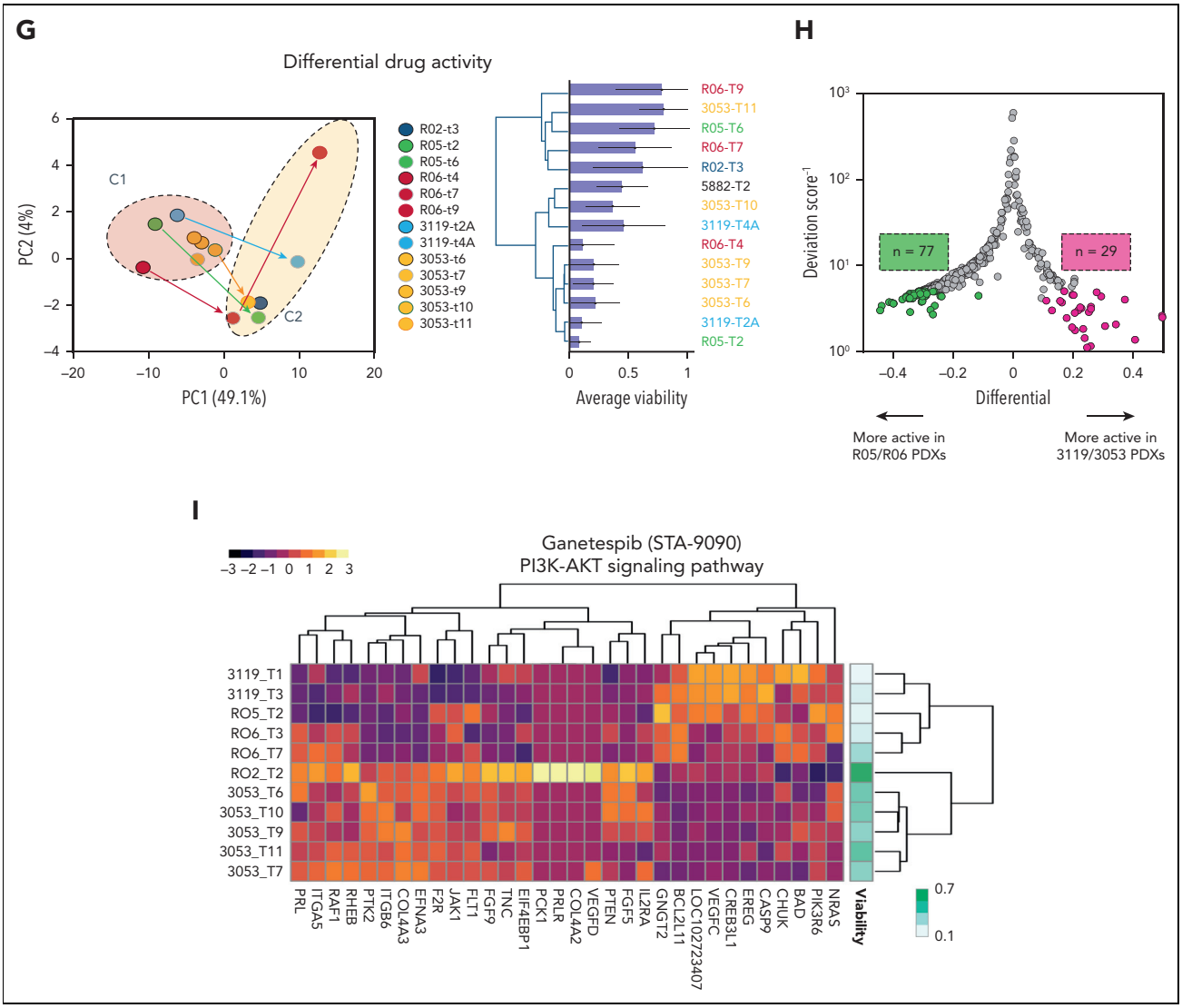

Figure 1 (continued) exposed to 433 drugs with in silico processing and analysis. (E) Dot plot showing drug responses as a function of media for 2 consecutive in vivo passages (RPMI with 10% FCS vs StemSpan [SS] with 10% KSR and interleukins) for a representative PDX (3053 T-ALL model). (F) Heat map showing the overall responses assessed using an ATP-Glo assay (Promega) of 6 different PDXs (14 samples corresponding to multiple passages) across 433 drugs screened in SS for 72 hours in duplicate (red, hits—low viability; white, viabilities greater than or equal to vehicle control). Dendrograms (left and bottom) show the unsupervised hierarchical clustering of drugs and PDX samples along the axis of maximum variation (Ward) of the Euclidean distances. The bar plot (top) shows the pan-drug viabilities per sample across all 433 drugs, with error bars highlighting the standard deviation. Bar plot (right) shows the pan-sample viability per drug, with the gray trend line highlighting the magnitude of the coefficient of variance. The orange inset highlights a subset of the 39 most active drugs across all PDX models, listed on the right panel with average viabilities shown as a bar plot and error bars showing the standard deviation. (G) PCA of 14 PDX samples based on the responses to all 433 drugs in the screening library (left). Dendrogram for the same samples shows unsupervised clustering based on the responses of the drug screening library (right). Two components (C1 and C2) were identified, corresponding to increased resistance of T-ALL cells with passaging over time in mice. (H) Volcano plot showing differential viability vs the inverse deviation score, highlighting differentially active drugs in RO5/RO6 vs 3119/3053 T-ALL PDX models. Green dots (left) indicate drugs more active in R05/RO6; magenta dots (right) denote drugs that are more active in 3119/3053 T-ALL models; gray dots indicate equally active drugs. (I) Heat map and unsupervised clustering depicting gene expression within the PI3K/AKT signaling pathway, targeted by HSP90 inhibitor ganetespib. Genes were selected on the basis of a significant correlation between their expression across samples and the viability of the treated sample. The viability values are indicated in the color bar (right). HSP90, heat shock protein90; PI3K/AKT, phosphatidylinositol-3-kinase/protein kinase B.

or R version 4.0 (released in 2020; R Foundation for Statistical Computing).

Results

Drug screening of T-ALL PDX cells identifies targetable vulnerabilities

We first characterized the transcriptomic profile of 39 T-ALL patient samples (Figure 1A), from which we established a library of PDX models (n = 22) (supplemental Table 1; supplemental Figure 1A-C). These closely recapitulated the transcriptomic profile and shared the identical T-cell receptor with those of matched patients (Figure 1B-C; supplemental Figure 1D; supplemental Table 1).

We then implemented a multistep approach, including (1) optimizing T-ALL PDX cell culture conditions ex vivo, (2) screening a broad library of drugs, (3) testing drug candidates in an EC-based coculture system, and (4) confirming key candidates in vivo using PDX models.

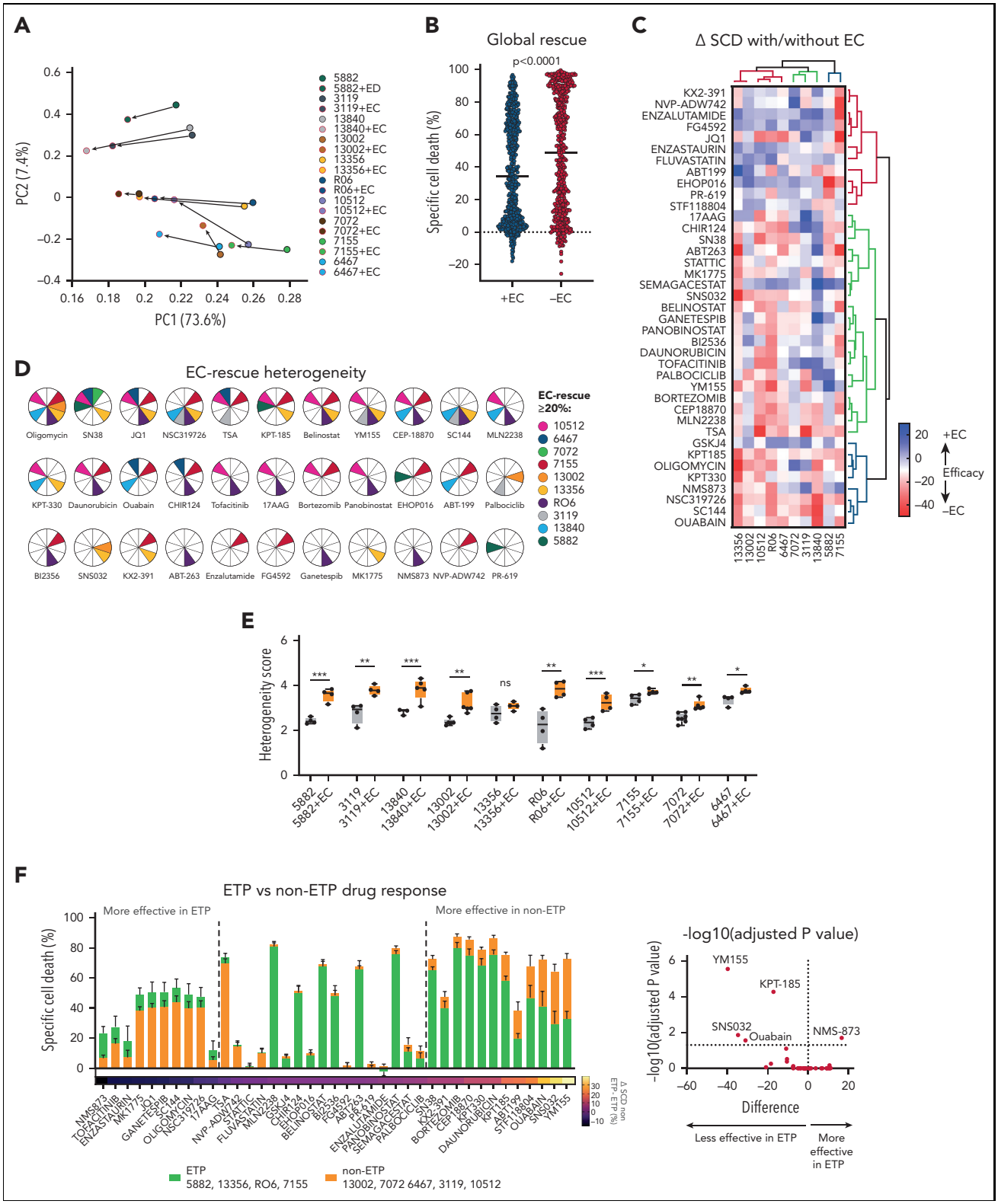

Figure 2. ECs provide protumorigenic signals to T-ALL cells. (A) Principal component analysis (PCA) plot showing the responses of 10 individual T-ALL PDX models cultured with and without ECs connected by vectors depicting the trajectory of the EC rescue. (B) Scatter plot showing the differential specific cell death between samples cocultured with E4-ECs vs alone for the 10 models from panel A. *P* value was estimated by *t* test. (C) Heat map showing the differential responses of 10 T-ALL PDX models in the presence or absence of ECs. Color coding corresponds to the change (delta) in specific cell death (SCD) of the +EC minus the –EC conditions (here referred to as efficacy ± EC). Red indicates drugs that are rescued by ECs; blue indicates those that produce more death in the presence of ECs. (D) Pie charts indicating the drugs having greater than 20% EC-mediated rescue for the 10 T-ALL PDX models. (E) Box-and-whisker plots showing the heterogeneity score (calculated as a modified Shannon entropy) per T-ALL PDX model in the presence or absence of ECs. (F) Box plot showing specific cell death (SCD) on exposure to the 39 most active compounds from the library in either ETP (yellow bars) or non-ETP (gray bars) models (median and standard error). Middle: Drugs that are equally effective between the 2 subgroups. Left: Drugs that are more efficient in ETP T-ALL. Right: Drugs that are more efficient in non-ETP T-ALL. The Δ SCD is color-coded at the bottom of the bars. Inset: Volcano plot of the same data, depicting $-\log_{10}$ *P* value corrected for multiple comparison (y-axis) and Δ SCD of ETP minus non-ETP samples. Top left corner: Drugs that are significantly less effective in ETP. Top right corner: Drugs that are significantly more effective in ETP models. ns, not significant.

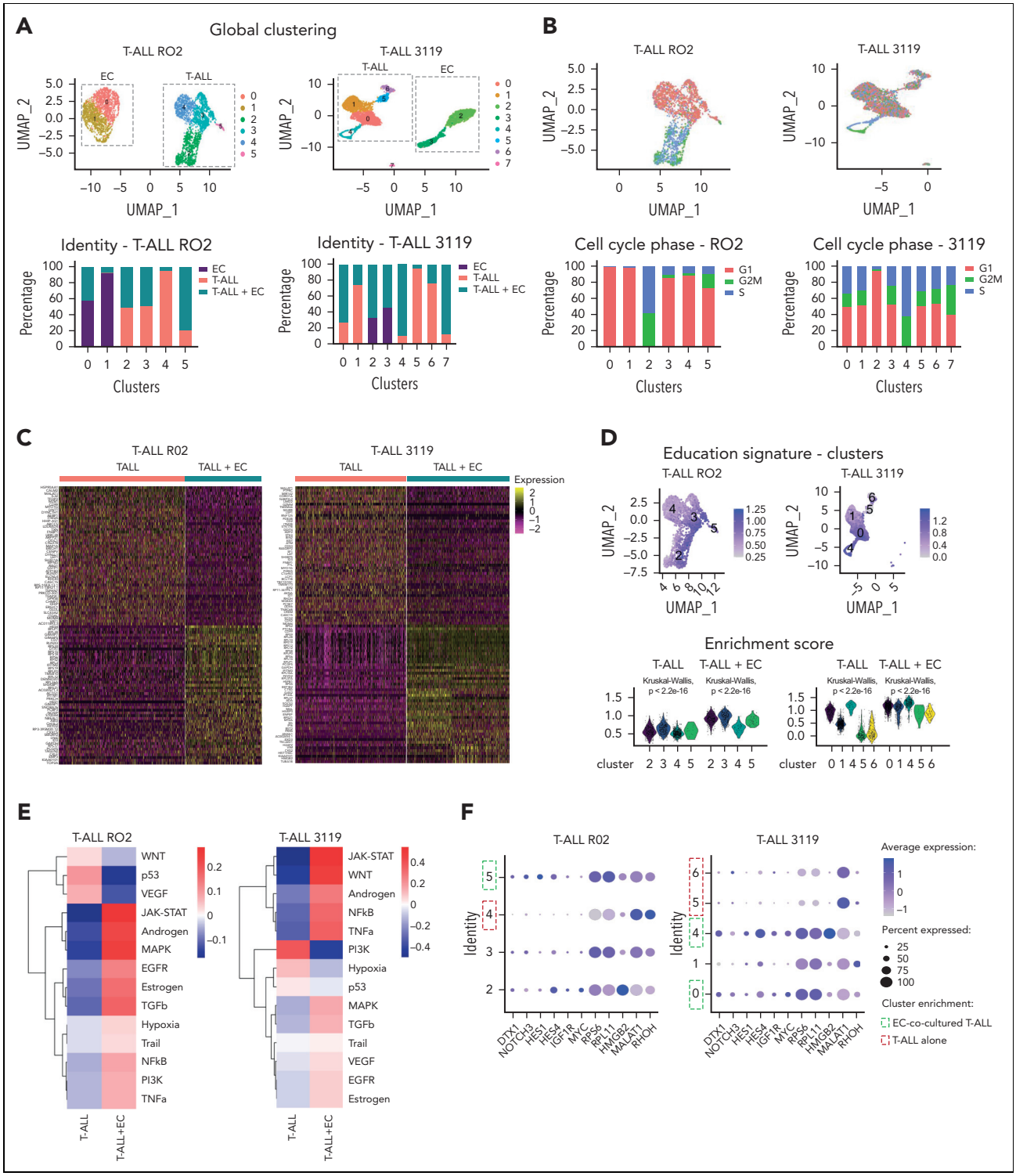

Figure 3. T-ALL cells are modulated by E4-ECs in vitro. (A) UMAP plots and cell clustering of single-cell RNA-Seq of T-ALL cells and E4-ECs. Freshly isolated T-ALL PDX cells were cultured alone or with E4-ECs. Single-cell RNA-Seq was performed on day 5. Top: Panels are color-coded by cluster identity. Bottom: Panels depict bar plots of sample identity in each cluster. (B) Top: UMAP plots of single-cell RNA-Seq of T-ALL cells color-coded by cell cycle (G_1, S, and G_2M phase). Bottom: Bar plots showing the different proportions of cells in G_1/S/G_2M phase based on cluster identity for both RO2 and 3119 T-ALL PDX models. (C) Heat map showing the differentially expressed genes from single-cell RNA-Seq of RO2 and 3119 T-ALL model cultured either alone or with E4-ECs. The top 50 up- and downregulated genes are depicted for each model. (D) UMAP and violin plots displaying T-ALL "education scores" calculated on the basis of differentially expressed genes from panel C. The scores are applied to each cluster to identify those with an enrichment in "educated" T-ALL cells. (E) Heat map depicting the pathway activity levels determined using the PROGENy tool applied on single-cell RNA-Seq data of RO2 and 3119 T-ALL cells cultured alone or in coculture with E4-ECs. (F) Dot plot displaying expression levels of a selected set of genes across different single-cell clusters composed of RO2 and 3119 T-ALL PDX cells cultured alone or with E4-ECs. The size of the dot indicates the percentage of cells expressing each gene, color-coded by expression level. Expression levels were measured using log-normalized counts. Green squares indicate clusters enriched for EC-cocultured T-ALL elements; red squares indicate clusters mainly consisting of T-ALL cultured alone. (G) Dot plot depicting expression levels of a signature of genes involved in T-cell maturation and commitment in T-ALL cells from RO2 or 3119 cultured with/without E4-ECs (from Park et al[51] and Le et al[52]). The size of the dot indicates the percentage of cells expressing each gene,

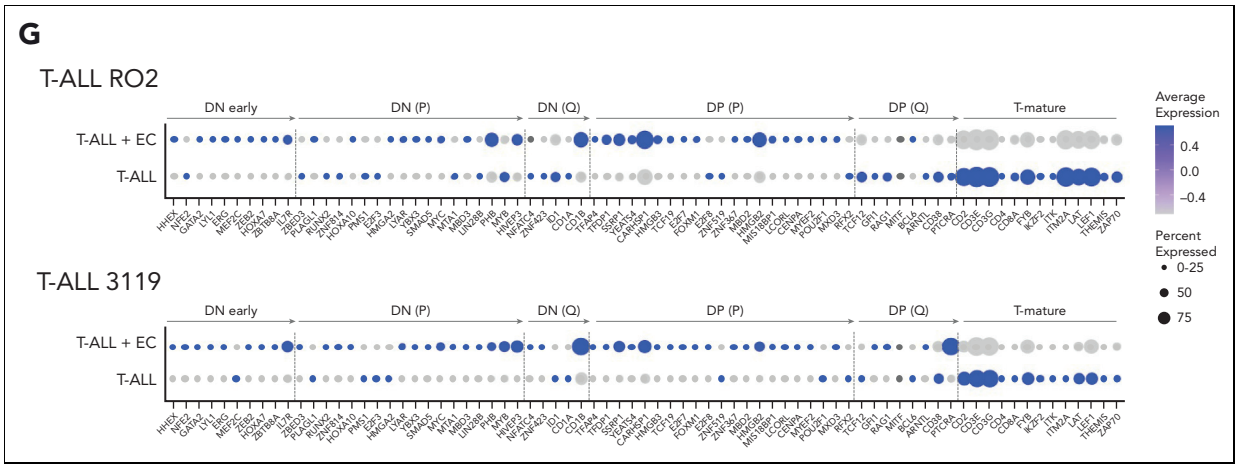

Figure 3 (continued) color-coded by expression level. Expression levels were measured using log-normalized counts. DN early, double-negative ($CD4^-/CD8^-$) early T cells; DN (P), double-negative proliferating T cells; DN (Q), double-negative quiescent T cells; DP (P), double-positive proliferating T cells; DP (Q), double-positive quiescent T cells; NFkB, nuclear factor κB; TRAIL, TNF-related apoptosis-inducing ligand; VEGF, vascular endothelial growth factor; UMAP, uniform manifold approximation and projection.

First, we tested various culture conditions and media, demonstrating improved viability and increased cell number in supplemented SS medium relative to supplemented RPMI medium (supplemental Figure 1E).

Second, we challenged T-ALL PDX cells ex vivo with a drug library of 433 compounds (1 μM), targeting ~634 proteins (Figure 1D,F; supplemental Table 2). Prior to choosing the 1 μM final concentration, we verified that the 50% inhibitory concentration (IC_{50}) would be reached in most of the compounds (400 of 433; 92%). In detail, 13 samples spanning different passages of 6 T-ALL PDX models were tested. We observed high reproducibility among biological and technical replicates (supplemental Figure 1F-I). SS-cultured PDX cells showed that most compounds (~89%) had little to no effect on T-ALL viability. Meanwhile, only 11% of drugs reduced average cell viabilities across the PDX models to less than 50%, corresponding to a cluster of 39 drugs (Figure 1F). To further elaborate on the drug concentration (1 μM), we tested serial dilutions of 10 of 39 broadly active compounds in 4 additional PDX models, identifying unique IC_{50} values in individual models (supplemental Figure 1P). In all cases, 1 μM was compatible with the efficacy range.

Using unsupervised hierarchical clustering and principal component analysis (PCA), we identified 2 clusters of T-ALL samples based on differential drug susceptibility (Figure 1G). Specimens belonging to earlier passages populated cluster 1 (C1), whereas later passages were more often skewed toward cluster 2 (C2), suggesting decreased therapeutic efficacy along serial passages (supplemental Figure 1I). We confirmed this reduced viability along serial passages using the 3053 T-ALL PDX (supplemental Figure 1J), in which the enrichment of the SMCHD1-JAK2 fusion overtime was observed (supplemental Figure 1K-M). To describe the response heterogeneity among the different T-ALL models, we combined the viability results of the 3119/3053 and R05/RO6 T-ALL PDXs based on the highest response similarity scores (supplemental Figure 1N) identifying differentially active drugs between the 2 groups (Figure 1H; supplemental Figure 1O). Last, we associated gene expression profiles with drug responses, to identify putative drug-related biomarkers. Despite the limited number of samples, we discovered several gene signatures linked with drug responses (Figure 1I; supplemental Figure 1Q-R).

Endothelial cells provide prosurvival signals and modulate drug response of T-ALL cells

Within the tumor microenvironment, endothelial cells (ECs) by supplying angiocrine factors sustain hematopoietic and neoplastic cells[36,37] and enhance their survival under toxic stress.[17,18,25,38,39] We previously demonstrated that primary nontransformed E4ORF1-transduced ECs[32] (herein referred to as E4-ECs) are an instructive serum-free/xenobiotic-free model to study tumor-host interactions.[25] Here, we first showed that E4-ECs sustained T-ALL cells under stress conditions such as starvation, lymphokine depletion, and oxygen deprivation (supplemental Figure 2A-E). We then developed a high-throughput flow cytometry–based endothelial-leukemia coculture system. Violet tracer–labeled T-ALL cells from 10 PDX models were cultured in SS medium supplemented with 10% KSR and challenged with the most effective drugs (n = 39) from the initial screening (n = 433) in the presence of CFSE-labeled E4-ECs (supplemental Figure 2F).

Sensitivity data showed a high concordance among T-ALL cells isolated from separate compartments (spleen and bone marrow) from the same PDX mouse (supplemental Figure 2G), from sibling mice implanted with the same tumor seeds (supplemental Figure 2H), and from mice belonging to 2 consecutive passages (supplemental Figure 2I). In addition, the percentage of viable E4-EC cells cultured alone and/or with T-ALL cells was similar across all compounds (supplemental Table 5). These findings suggested that T-ALL responses likely were not linked to suboptimal drug concentrations (supplemental Figure 2J).

Overall, E4-ECs significantly improved the T-ALL survival of individual PDX models against selected compounds after 72 hours of ex vivo treatment (Figure 2A-D; supplemental Figure 2K). A compound was defined as "rescued" when there

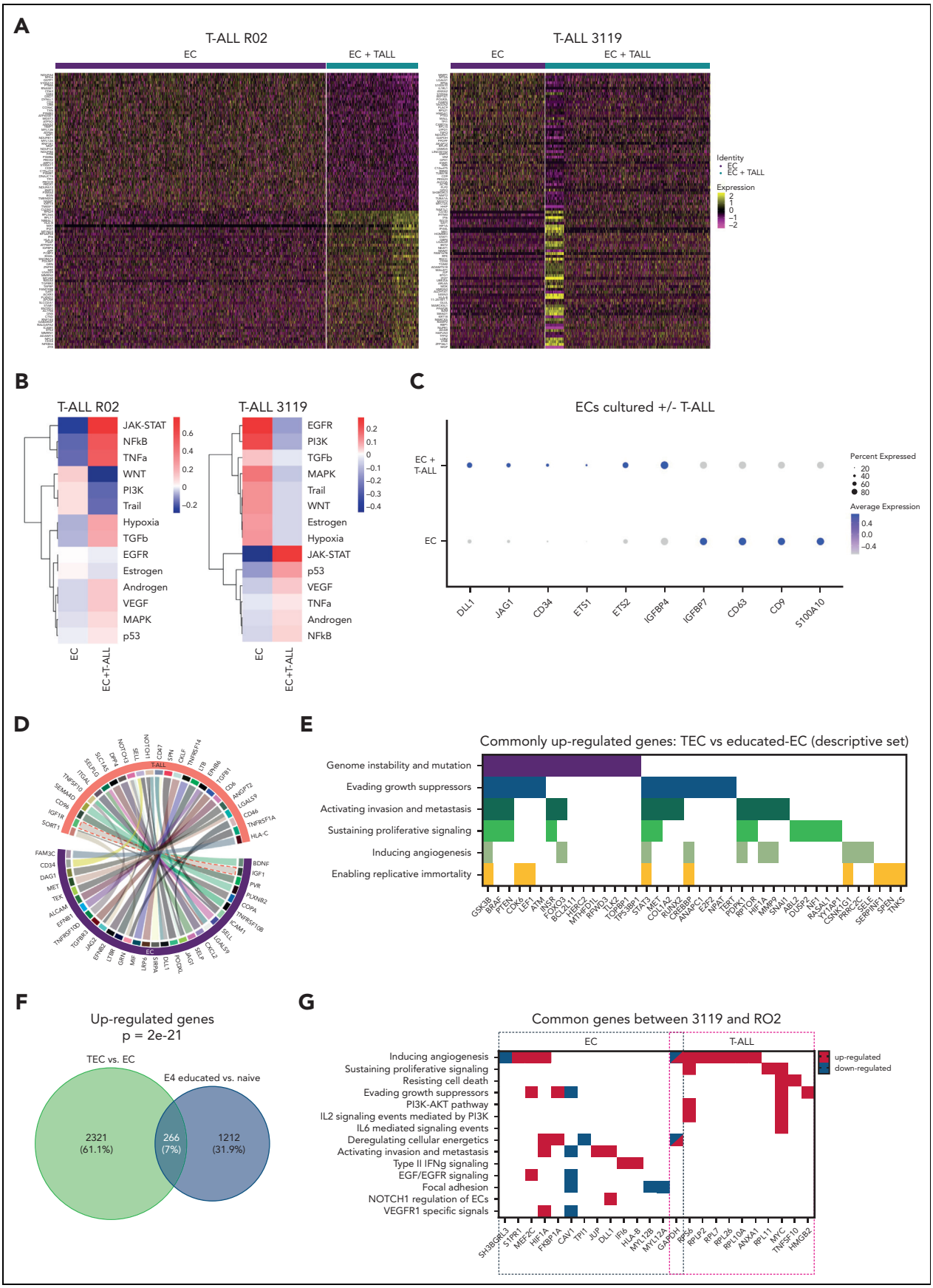

Figure 4. E4-ECs in contact with T-ALL establish a maladapted niche and acquire TEC-like features. (A) Heat map of the top 50 up- and downregulated genes from single-cell RNA-Seq in ECs alone or after coculture with T-ALL elements in both RO2 and 3119 PDX models. (B) Heat map depicting the pathway activity levels determined using the

was a decrease of at least 20% in specific cell death compared with the no-EC condition. By PCA, the vectorized EC rescue showed converging directions in all models, suggesting conserved rescue mechanisms (Figure 2A-B; supplemental Figure 2K). Of note, some compounds were reproducibly rescued across multiple PDX models (including oligomycin, JQ1, NSC319726, SN38, belinostat, CEP-18870, KPT-185, SC144, TSA, and YM155). Others were poorly effective in specific models, underlying potential "private" rescue mechanisms (Figure 2C-D; supplemental Figure 2L-M). Further, we tested 12 additional drugs on 7 of 10 PDX models screened, including conventional chemotherapeutics for T-ALL and novel compounds in clinical trials (supplemental Figure 2N). We identified commonly rescued drugs: asparaginase, dexamethasone, vincristine, ponatinib, dasatinib, and YKL-5-124 (CDK7 inhibitor) in 4 models. Overall, rescued compounds were active on molecules belonging to interconnected pathways, such as PI3K/AKT, p53, FoxO, JAK/STAT, NOD-like receptor, and HIF-1 (supplemental Figure 2M). Next, we computed a modified Shannon entropy for each PDX model (see "Methods") (Figure 2E), showing an overall tendency toward increased response heterogeneity and plasticity in the presence of E4-ECs. We then focused on the different response profiles of the 10 PDX models challenged in the presence of E4-ECs. Among the most effective drugs across all models, some are of particular interest because of their potential clinical applicability: proteasome inhibitors (bortezomib, CEP18870, and MLN2238; average specific cell death [SCD]: 83%, 79%, and 78%, respectively), histone deacetylase (HDAC) inhibitors (panobinostat, belinostat, and CHIR124; average SCD: 75%, 69%, and 51%, respectively), heat shock protein (HSP)-90 inhibitor (ganetespib; average SCD, 49%), and BCL2 inhibitors (venetoclax and navitoclax; average SCD: 27% and 66%, respectively). Notably, other drugs displayed unique efficacy in selected models and against different T-ALL phenotypes, with ETP-ALL samples showing increased resistance to several compounds (Figure 2F; supplemental Figure 2O-R): YM155 (survivin inhibitor; Δ SCD [ETP – non-ETP] = 39.9%; $P < .0001$), SNS032 (CDK2/9 inhibitor; Δ SCD = 34.7%; $P = .01$), ouabain (ATP1A1 inhibitor; Δ SCD = 31%; $P = .02$), STF118804 (nicotinamide phosphoribosyltransferase [NAMPT] inhibitor; Δ SCD = 20.9%), and KPT-185 (exportin 1 [XPO1] inhibitor; Δ SCD = 17.2%; $P < .0001$).

Finally, we used our dual T-ALL-EC platform to test targets based on the genetic background of individual T-ALL PDXs. We treated the 3119 PDX cells (carrying a *NUP14/ABL* translocation) with dasatinib, and RO2 PDX cells (mutant *JAK1-JAK3-STAT5B*) and RO6 PDX cells (mutant *STAT5*) (supplemental Table 1) with Jak inhibitors (ruxolitinib and tofacitinib, alone or in combination), in the presence or absence of E4-ECs (supplemental Figure 2S). E4-ECs partially rescued T-ALL cells from single-agent treatments. However, in combination, ruxolitinib and tofacitinib were significantly more effective in both RO2 and RO6 PDXs.

These results highlighted the utility of the T-ALL-EC platform to assess (1) drugs that are effectively rescued by ECs, (2) pathways collectively or privately involved in EC rescue, (3) differential T-ALL response profiles based on intrinsic tumor features, and (4) unique targetable T-ALL vulnerabilities.

T-ALL cells and ECs reciprocally modulate their transcriptomes

Aiming to elucidate the relationships between ECs and T-ALL cells, we investigated the transcriptomic profiles of cocultured E4-ECs and T-ALL cells from 3119 and RO2 PDX models, using single-cell RNA sequencing (scRNA-Seq). After quality control filtering (supplemental Figure 3A), we clustered all cells on the basis of the most variable genes (Figure 3A; supplemental Figure 3B-D), and analyzed the 3119 and RO2 T-ALL PDX models separately, given their divergent genetic profiles (supplemental Table 1). Notably, proliferating T-ALL cells were most frequently included in clusters enriched in EC-cocultured T-ALL cells in both models (Figure 3B; supplemental Figure 3E). We found that T-ALL cocultured with E4-ECs underwent profound transcriptional changes (Figure 3C; supplemental Table 6). Furthermore, the differentially expressed genes defined an "EC-mediated T-ALL education signature" for each model, with significant overlap between the 2 models and a high concordance with bulk RNA-Seq data from cells cultured under the same conditions (Figure 3D; supplemental Figure 3F-G). In addition, we detected enhanced single-cell entropy in T-ALL cocultured with E4-ECs (supplemental Figure 3H), accounting for increased plasticity.[40,41]

Then, we compared differential pathway activation between the 2 conditions. Both EC-cocultured RO2 and 3119 T-ALL cells upregulated JAK/STAT, mitogen-activated protein kinase (MAPK), transforming growth factor-β (TGFB), and epidermal growth factor receptor (EGFR) pathways, with downregulation of the p53 signaling pathway (Figure 3E). Gene set enrichment analysis (GSEA) showed enrichment of the c-Myc pathway in cocultured elements (supplemental Figure 3I), along with increased expression of genes belonging to the NOTCH pathway (*NOTCH3*, *HES1*, *HES4*)[42,43] (Figure 3F). Notably, insulin-like growth factor 1 receptor (*IGF1R*) was also commonly upregulated in cocultured T-ALL cells in both models (Figure 3F; supplemental Figure 3J). Other commonly upregulated genes included ribosomal genes *RPS6* (highly expressed in several solid cancers[44] and in immature leukemic blasts),[45]

Figure 4 (continued) PROGENy tool applied to single-cell RNA-Seq data of E4-ECs cultured alone or in coculture with 3119 and RO2 T-ALL cells. (C) Dot plot displaying expression levels for a set of genes of interest (*DLL1*, *JAG1*, *CD34*, *ETS1*, *ETS2*, *IGFBP4*, *IGFBP7*, *CD63*, *CD9*, and *S100A10*) in E4-ECs that were cultured alone or in coculture with RO2 and 3119 T-ALL elements. The dot size encodes the percentage of cells expressing each gene, and the color encodes the average expression level across all cells. Expression levels were measured using the log-normalized counts. (D) Circos plot of ligand-receptor interaction obtained through the CellPhoneDB package on the RO2 PDX model, based on the relative expression level measured by single-cell RNA-Seq. Only the significant associations between ligands and receptors (on either the T-ALL or the EC side) are depicted. (E) List of a set of genes commonly upregulated by tumor endothelial cells (TECs) (vs normal ECs) and by E4-ECs cocultured with T-ALL cells (vs cultured alone) (see panel F). The list of processes and functions involving each gene was derived from the NDEx Biological Network Repository. (F) Venn diagram showing a comparison of genes upregulated in TECs vs normal E4-ECs (green circle) and in educated vs naive E4-ECs (blue circle). *P* value was calculated using a hypergeometric test. (G) List of a set of genes up- or downregulated by E4-ECs and T-ALL cocultured vs cultured alone in common between the 2 PDX models (RO2 and 3119) (supplemental Figure 4I). The direction of the differences is color-coded (blue, downregulated; red, upregulated). The list of processes and functions involving each gene was derived from the NDEx Biological Network Repository. IL-2, IL-6, interleukins 2 and 6.

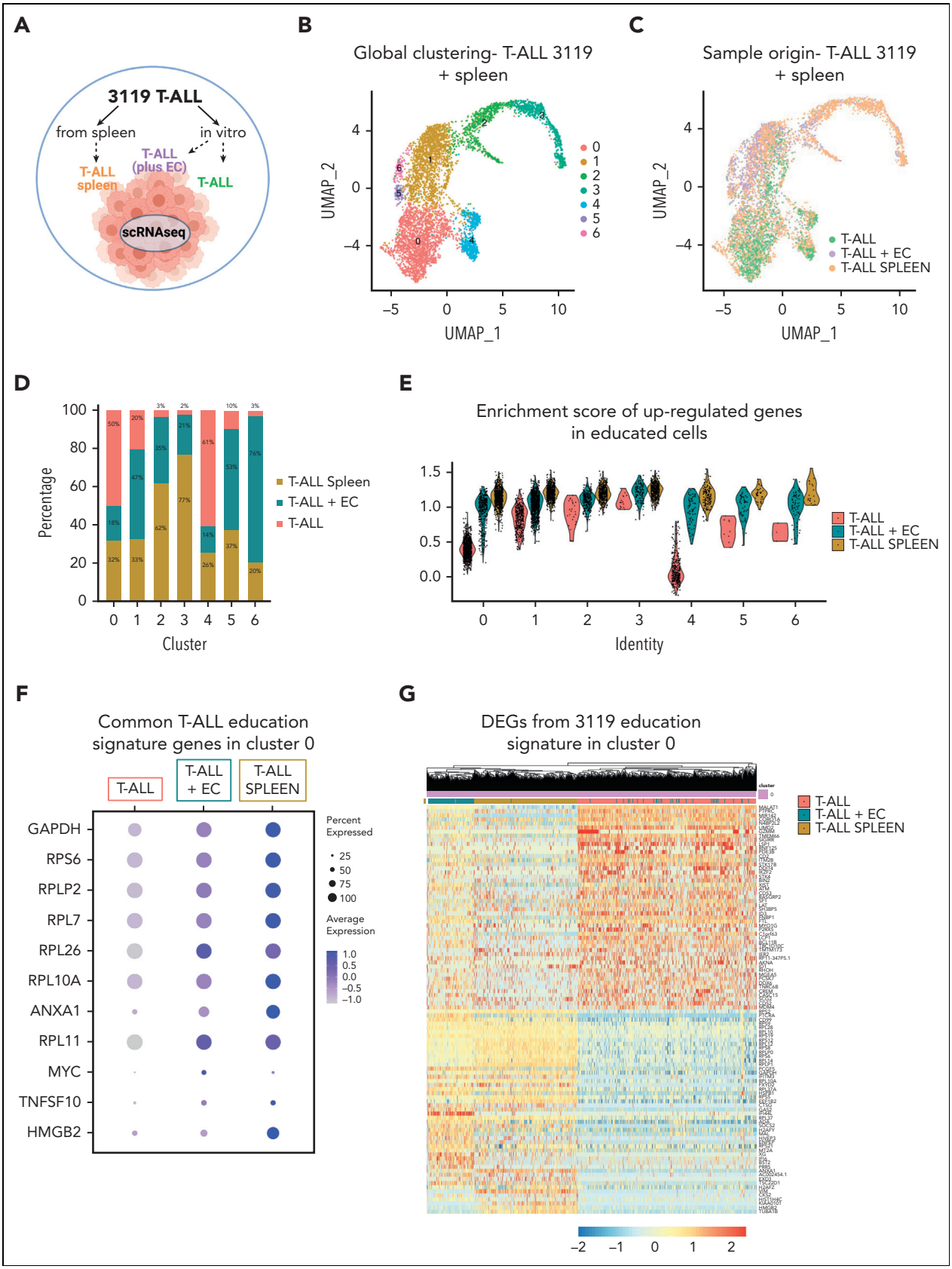

Figure 5. In vitro EC-cocultured T-ALL cells mirror in vivo T-ALL cells. (A) Schematic representation of the single-cell RNA-Seq analysis of 3119 T-ALL cells. Cells that were either cultured alone or cocultured with E4-ECs in vitro for 5 days were sequenced and combined with T-ALL cells freshly harvested from the spleen of a 3119 PDX mouse. (B) UMAP plot of the single-cell RNA-Seq data derived from panel A, color-coded by cluster identity. (C) UMAP plot of the single-cell RNA-Seq data derived from panel A, color-coded by sample origin. (D) Bar plot showing the proportions of in vitro and in vivo T-ALL cells (panel A) based on cluster identity. (E) Violin plots showing the enrichment score

RPL11 (whose activating mutations have been described in T-ALL),[46] and *HMGB2*, a known poor prognostic factor in several cancers.[47,48] In both models, *MALAT1* (known to control the crosstalk between ECs and tumor cells[49]) was identified as one of the most downregulated genes in E4-EC-cocultured T-ALL. Similarly, *RHOH*[50] (Figure 3C,F), normally expressed in hematopoietic cells where it functions as a negative regulator of cell growth and survival, was also downregulated. Importantly, these differences were maintained at single-cell resolution, allowing us to define model-specific clusters with enrichment of educated cells (RO2, cluster 5; 3119, clusters 0 and 4) (Figure 3F). Finally, to investigate whether E4-ECs could contribute to preserving a more immature/stemlike phenotype, we evaluated the differential expression of genes linked to T-cell commitment and maturation.[51,52] In both models, EC-cocultured T-ALL cells expressed higher levels of genes related to early double-negative (DN) or double-positive proliferating (DP-P) thymocytes. In contrast, T-ALL cells cultured alone were shifted more toward DP-quiescent (Q) or mature T-cell phenotypes (Figure 3G).

ECs in contact with T-ALL acquire maladapted TEC-like features

We then focused on the transcriptomes of E4-ECs cultured alone or with T-ALL cells of the 3119 and RO2 PDX models. Overall, we distinguished different clusters corresponding to T-ALL-cocultured ECs (educated E4-ECs) or E4-ECs cultured alone (Figure 4A; supplemental Figure 4A). These populations were transcriptionally distinct, leading to the construction of T-ALL-mediated "EC education signatures" (Figure 4A; supplemental Table 7). Globally, cocultured E4-ECs upregulated interferon-γ and -α response hallmark pathways (supplemental Figure 4B) and increased the activity of multiple pathways, including JAK/STAT, nuclear factor-κB (NF-κB), tumor necrosis factor-α (TNF-α), and vascular endothelial growth factor A (VEGF-A) (Figure 4B), with a concurrent increase in entropy reflecting in higher differentiation potency and plasticity (supplemental Figure 4C).[40,41] At the gene level, cocultured E4-ECs displayed enrichment in Notch signaling, angiogenesis (*DLL1*,[53] *JAG1*,[54] and *CD34*), cell migration, and survival (*ETS1*, *ETS2*, and *IGFBP4*) genes (Figure 4C). Conversely, *IGFBP7*, a known IGF1R decoy with tumor suppression features in different cancer types;[55] *CD63/TIMP-1* (involved in endothelial migration); *CD9*; and *S100A10* (regulating cell-cell interaction) were downregulated in cocultured E4-ECs (Figure 4C).

We then performed a ligand-receptor analysis in the 3119 and RO2 PDX models to investigate the bidirectional crosstalk between T-ALL and E4-ECs (Figure 4D). This approach led to the identification of heterogeneous interactions, mainly coshared by the 2 models (Figure 4D; supplemental Figure 4D). Among them, the IGF1-IGF1R axis was significantly enriched (outlined in red in Figure 4D). Because cocultured T-ALL upregulated *IGF1R*, and conversely E4-ECs downregulated *IGFBP7* (see above), we attempted to functionally verify whether the selective abrogation of the IGF1 pathway could impact the EC-mediated drug rescue. We tested the 39 pan-effective drugs (Figure 2C) with or without the recombinant IGFBP7 (500 ng/mL) in the 3119 and 3053 PDXs. Of note, IGFBP7 abrogated the E4-EC-mediated rescue of enzastaurin (PKC-β inhibitor) and SC144 (GP130 inhibitor) in T-ALL PDX 3119 and 3053 models, and CHIR124 (Chk1 inhibitor) and YM155 (survivin inhibitor) in T-ALL PDX 3119 (supplemental Figure 4E). As these drugs regulate the activity of IGF1R or its downstream effectors[56-58] (supplemental Figure 4F), we postulate that the EC-mediated rescue is in part mediated by the engagement of IGF1R of T-ALL cells.

To further explore the changes in T-ALL-cocultured E4-ECs, we correlated their transcriptomics profiles with tumor ECs (TECs—directly sorted from tumor masses) and naive normal/E4-ECs (supplemental Table 8). These analyses demonstrated that in vitro educated E4-ECs and TECs share a set of differentially expressed genes, relative to normal E4-ECs (Figure 4E-F; supplemental Figure 4G-H). These genes have been implicated in orchestrating invasion and metastasis (ie, *GSK3B*, *BRAF*, *STAT3*, *MET*), genome instability (ie, *PTEN*, *BRAF*, *KEF1*, *ATM*), angiogenesis (ie, *FOXO3*, *CREBBP*, *HIF1A*), and enabling immortality (ie, *CDK6*, *SPEN*, *TNKS*).

Last, we looked for genes coshared by both RO2 and 3119 PDX models whose expression contributed to the education signatures in both compartments (EC and T-ALL) (Figure 4G; supplemental Figure 4I; supplemental Table 9). As expected, genes linked to the EC and T-ALL compartments were distinct and displayed different functional modules (Figure 4G). Therefore, the T-ALL-EC model is an informative and useful tool to probe EC-tumor interactions.

In vitro EC-educated T-ALL cells mirror in vivo T-ALL cells

To validate the data generated using the in vitro coculture platform, we performed scRNA-Seq on T-ALL cells from the 3119 PDX spleen (ex vivo splenic T-ALL cells). We identified 4 clusters representative of the intratumor heterogeneity based on the differential expression of genes related to: cell cycle, MYC, PI3K/AKT signaling, and epithelial-mesenchymal transition (supplemental Figure 5A-C). Then, we enriched our analysis by including cells from the same source cultured for 5 days ex vivo in SS medium either with E4-ECs (in vitro EC-educated T-ALL) or without E4-ECs (T-ALL alone) (Figure 5A). Overall, 7 T-ALL cell clusters were identified (Figure 5B-C). Clusters 0 and 4 were enriched with T-ALL elements cultured without ECs; clusters 1, 5, and 6 with T-ALL cultured with ECs; and clusters 2

Figure 5 (continued) of the education signature derived from the in vitro experiment with the 3119 PDX model (Figure 3D). In vitro EC-cocultured and splenic T-ALL cells displayed similar enrichment across all clusters. (F) Dot plot displaying expression levels for a set of genes in common between RO2 and 3119 T-ALL "educated" elements (Figure 4G, T-ALL genes) in ex vivo splenic T-ALL cells compared with in vitro T-ALL elements (E4-ECs cocultured and cultured alone). The expression of these genes was very similar in splenic and E4-EC-cocultured T-ALL cells compared with T-ALL cultured alone, demonstrating that in vitro EC-educated elements are more similar to those freshly harvested ex vivo. The dot size encodes the percentage of cells expressing each gene, and the color encodes the average expression level across all cells. Expression levels were measured using the log-normalized counts. (G) Heat map of the genes from the 3119 "education signature" (Figure 3D) applied to cluster 0 from panel B containing enough cells from all 3 compartments (in vitro T-ALL cultured alone vs with E4-ECs and ex vivo splenic T-ALL). Cell proportions in cluster 0 are found in panel D. T-ALL cells from the spleen are clustered together with EC-cocultured T-ALL cells, based on the expression of the education signature. DEG, differentially expressed genes.

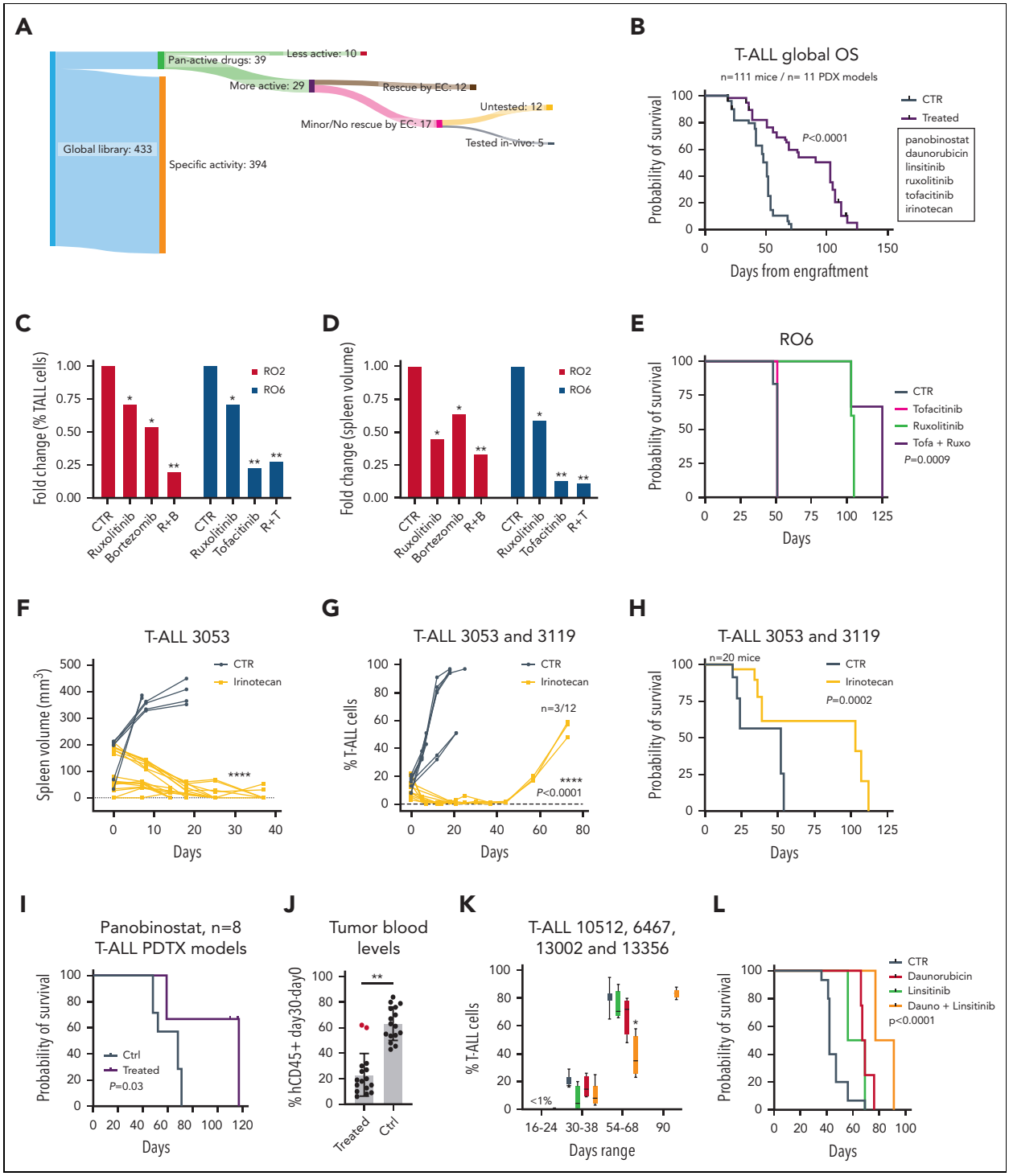

Figure 6. Efficacy of positive hits from stepwise drug discovery approach in vivo. (A) Representative scheme of our stepwise drug discovery approach coupled with in vivo preclinical trials. Tumor cells from T-ALL PDXs were first screened with a library of 433 compounds in 384-well plate format. Positive hits were then validated in 96-well plate format with and without E4-ECs. The number of candidates was narrowed down (n = 29) after implementation of multiple experimental conditions and validations. Representative drugs not rescued by E4-ECs were then tested in vivo and proved to be effective in T-ALL PDX mice. (B) Kaplan-Meier plot depicting overall survival of all the mice (n = 111) treated with vehicle vs different therapeutic regimens across 11 different PDX models. *P* value was calculated using a log-rank test. (C) Bar plot showing the fold change in the percentage of T-ALL cells in the blood of RO2 and RO6 PDX mice treated with ruxolitinib, bortezomib, tofacitinib, and combinations compared with controls. *P* values were calculated by *t* test. **P* < .05; ***P* < .01. (D) Bar plot showing the fold change in the spleen volume (measured by MRI) of RO2 and RO6 mice treated with ruxolitinib, bortezomib, tofacitinib, and combinations compared with controls. *P* values were calculated by *t* test. **P* < .05; ***P* < .01. (E) Kaplan-Meier plot depicting overall survival of RO6 mice treated with vehicle, tofacitinib, ruxolitinib, or combination. *P* value was calculated using a log-rank test. (F) Line-dot plot showing changes in spleen volume (measured by MRI) of 3053 PDX mice treated with irinotecan (20 mg/kg per day) compared with controls in a timeframe of 40 days. *P* value was calculated by *t* test. *****P* < .0001. (G) Line-dot plot showing changes in percentage of T-ALL cells in blood of 3053 and 3119 PDX mice treated with irinotecan compared with controls in a timeframe of 80 days. Three of the 12 irinotecan-treated mice relapsed and died of leukemia. *P* value was calculated by *t* test. *****P* < .0001. (H) Kaplan-Meier plot depicting overall survival of 3053 and 3119 PDX mice treated with vehicle or irinotecan. Nine of the 12 irinotecan-treated mice died without leukemia. *P* value was calculated using a log-rank test. (I) Kaplan-Meier plot depicting overall survival of 8 different T-ALL PDX models (6467, 14741, 7072, 7155, 13002, 13356, 10512, and 5384) treated with vehicle or HDAC inhibitor panobinostat (n = 2

and 3 with T-ALL cultured from spleen. Of note, clusters 2, 3, 5, and 6 showed a great abundance of E4-EC-educated T-ALL or spleen T-ALL cells (Figure 5D), pointing to the closer similarity of these 2 compartments compared with cultured alone T-ALL cells. Notably, clusters 2 and 3 were highly enriched for proliferating cells (supplemental Figure 5D). Then, we applied the T-ALL education signature defined in the previous in vitro experiment within each cluster (Figure 5E). Remarkably, in vivo splenic T-ALL were globally more similar to in vitro EC-educated T-ALL than T-ALL alone. This was more evident in clusters 0 and 4, containing enough cells belonging to all different entities (Figure 5F-G; supplemental Figure 5E). Ultimately, splenic T-ALL cells recapitulated the different expressions of genes contributing to the education signatures of both 3119 and RO2 PDX models (Figure 5F-G; supplemental Figure 5E). These data demonstrated the reliability of the EC/T-ALL coculture platform in recapitulating in vivo conditions.

Positive hits selected in vitro are effective in preclinical trials

To validate our stepwise drug screening platform in vivo, we selected 5 compounds shown to be effective on T-ALL cells in the presence of E4-ECs (Figure 2A-C; supplemental Figure 2O-P), effective in preclinical settings, and/or effective in targeting underlying PDX T-ALL vulnerabilities. Panobinostat (HDAC inhibitor), ruxolitinib (JAK1/2 inhibitor), tofacitinib (JAK1/2/3, TYK2 inhibitor), bortezomib (20S proteasome inhibitor), and irinotecan (topoisomerase I inhibitor) were tested in 11 PDX models, accounting for an overall number of 111 mice (Figure 6A-B). Overall, treated mice had a better prognosis than mice receiving vehicles (Figure 6B). First, R02 and R06 T-ALL PDX mice were challenged with ruxolitinib alone or in combination with bortezomib (RO2) or tofacitinib (RO6) (supplemental Figure 6A). Treatments were well tolerated, with no signs of toxicity (data not shown). In comparing treated and control mice, spleen size and percentage of leukemic circulating cells were significantly reduced (Figure 6C-D; supplemental Figure 6B-C). Among the 3 single agents tested, ruxolitinib was least effective in reducing circulating disease in both models, whereas both combinations allowed for better disease control, more pronounced reduction in spleen volumes, and improved overall survival (Figure 6C-E; supplemental Figure 6B-E). Based on the ex vivo coculture drug screening, we identified SN38 (the active metabolite of irinotecan) as active in all models, despite an insufficient partial rescue by E4-ECs (death rate of T-ALL cells, >50% compared with controls in all cases [mean SCD, 68%; range, 54%-83%]; Figures 1F and 2C). Accordingly, we randomized the 3053 and 3119 T-ALL PDX mice to receive either vehicle or irinotecan (20 mg/kg per day for 2 weeks) (supplemental Figure 6F). Total body MRI documented a normalized spleen size by day 15 in treated mice (Figure 6F). We also detected a reduced blood leukemia burden in treated mice up to 40 days and improved overall survival (Figure 6G-H) (median OS, 103 vs 52 days; $P = .0002$). No signs of overt toxicity were documented (supplemental Figure 6G).

Epigenetic targeting using the HDAC inhibitor panobinostat has been suggested as a potential therapy against T-ALL,[59] and this strategy was supported by our in vitro drug screening (Figures 1F and 2C). Thus, we executed a single-drug preclinical trial with panobinostat, in 8 different T-ALL PDX models (Figure 6I; supplemental Figure 6H). This treatment significantly improved OS (median OS, 117 vs 68; $P = .03$) (Figure 6I) and decreased circulating T-ALL blasts (Figure 6J). Last, based on the finding that the IGF1-IGF1R axis is upregulated in EC-cocultured T-ALL cells (Figures 3F and 4D; supplemental Figure 3J) and that its inhibition downregulated EC-mediated rescue (supplemental Figure 4E), we evaluated a selective IGF1R inhibitor (linsitinib) in vivo in 4 different PDX models (Figure 6K-L; supplemental Figure 6I). As a debulking agent, we used daunorubicin, an identified pan-active compound in our drug screening in vitro (Figures 1F and 2C). The combination of daunorubicin plus linsitinib controlled disease more effectively and improved OS (median, 84 days) compared with single agents (median: daunorubicin, 68 days; linsitinib, 63 days) or controls (median, 42 days) ($P < .0001$) (Figure 6K-L), suggesting that the IGF1-IGF1R inhibition counteracted leukemia progression in combination with standard chemotherapy.

These data demonstrated the predictive utility of our screening platform as a drug discovery process to identify active compounds and T-ALL dependencies.

Discussion

Our study presents a novel customized vascular niche/cancer platform to define targetable vulnerabilities and identify effective drugs against T-ALL cells, potentially applicable to other cancers. Although the treatment of patients with T-ALL has considerably improved, relapsed T-ALL often remains incurable.[5,6] Preclinical studies have provided encouraging approaches;[60-62] however, therapeutic response does not always depend on pathogenetic mutations,[10,63] and preclinical trials are costly and require specialized units. We envisioned a multistep approach that integrates readouts from large drug screenings on PDX cells ex vivo, followed by "ad hoc" in vivo cross-validation (Figure 6A). We first identified a group of broadly active compounds across all models tested and observed that increased drug resistance might arise along serial PDX propagations. This should be further exploited to improve our understanding of therapeutic failures. Of interest, we could find a correlation between responses and a priori transcriptional

Figure 6 (continued) mice per arm, n = 32 mice total) (5 mg/kg per day). Mice belonging to 3 of the 8 models (5384, 7155, and 6467) died without leukemia. *P* value was calculated using a log-rank test. (J) Bar plot depicting the circulating T-ALL cells (difference between day 30 and day 0; day 0: first T-ALL detection in the blood) in 8 PDX models treated with vehicle or panobinostat. A single partially refractory model was identified (1 of 8, 7072 PDX T-ALL). *P* value was calculated by *t* test. $^{**}P < .001$. (K) Bar plots depicting the percentage of circulating T-ALL cells in 4 PDX models (10512, 6467, 13002, and 13356) treated with vehicle, daunorubicin (1.2 mg/kg for 3 days/week), linsitinib (50 mg/kg per day), or combination (n = 2 mice per arm, n = 32 mice total). Mice treated with daunorubicin plus linsitinib displayed delayed leukemia progression compared with the other arms. *P* value was calculated by *t* test. $^{*}P < .05$. (L) Kaplan-Meier plot depicting overall survival of 10512, 6467, 13002, and 13356 T-ALL PDX models treated with vehicle, daunorubicin, linsitinib, or combination. Mice treated with daunorubicin plus linsitinib survived until 3 months from enrollment. *P* value was calculated using a log-rank test.

profiles for selected agents, a strategy that can provide new avenues to discover biomarkers predictive of responses.

It is well known that the tumor microenvironment can modulate drug responses in acute leukemia, a scenario epitomized by the contribution of mesenchymal and endothelial cells.[15-19] Specifically, ECs have been seldom used in broad drug discovery programs.[64] Nevertheless, their role in the maintenance/regulation of HSCs[36,37] is established, fostering ALL survival via a multitude of signaling pathways (ie, Notch,[65] SDF-1,[66] and CXCL12[67]). Accordingly, we generated a coculture system using E4ORF1-transduced ECs, which have been proven to sustain T-ALL cells in vitro and can be propagated for at least 5 to 10 passages in vitro. This system demonstrated that the T-ALL drug susceptibility was often downmodulated by ECs. Single-cell analysis revealed that a multitude of ligand-receptor interactions and downstream pathways are involved in this process (eg, IGF1/IGF1R, NOTCH-DLL, and JAK/STAT), suggesting that the EC-mediated prosurvival effect may require a multitargeted approach to be fully counteracted. Toward this end, adding recombinant IGFBP7 in vitro partially abrogated EC rescue for selected compounds, suggesting reliance on the IGF1-IGF1R pathway in specific cases.

On the other hand, several compounds were effective in the presence of ECs across multiple models. These included drugs with clinical interest (proteasome, HDAC, HSP-90, and BCL2 inhibitors). We also observed a degree of heterogeneity which may be partially linked to unique T-ALL subgroups, with ETP-ALL being overall more resistant, specifically on exposure to drugs targeting PI3K/AKT and JAK/STAT pathways. A selection of 5 compounds was ultimately shown to be effective in vivo either alone or in combination. This was exemplified by irinotecan, a drug currently approved for treating many solid tumors, suggesting its potential repositioning in the context of T-ALL, and panobinostat, an HDAC inhibitor whose effect in T-ALL has not been fully unraveled. Similarly, the efficacy of JAK/STAT inhibitors has been documented in models carrying activating mutations.[10,13,68] Moreover, the data generated in vitro with recombinant IGFBP7 and the improved survival of daunorubicin-treated T-ALL PDX in combination with IGF1R inhibitor linsinitib (although limited on 4 models) further support the role of IGF1-IGF1R signaling in the leukemia-EC crosstalk.

Mechanistically, we show that ECs and T-ALL cells undergo bilateral transcriptional changes modulating critical signaling pathways at single-cell resolution. On the T-ALL side, these genes were mostly linked to stemness, T-cell commitment, and maturation, emphasizing the heterogeneity and plasticity of leukemic elements. Remarkably, T-ALL cocultured with E4-ECs were more similar to ex vivo splenic T-ALL cells freshly harvested from PDX mice compared with T-ALL cells cultured alone, proving the reliability of our coculture system. On the EC side, a significant set of differentially expressed genes was expressed in common with in vivo TECs. These bidirectional changes are reflected in increased transcriptomic and pharmacological entropy, further pointing toward the dynamicity of this dual-culture system compared with conventional static single cell suspension cultures.

Hence, the EC/T-ALL coculture system partially recapitulates in vivo conditions, representing a robust platform to study leukemia-host interactions and drug sensitivities. We envision that this integrated stepwise approach might overcome the liabilities of current drug screenings and propel the entry of new agents and combinations in clinical trials.

Acknowledgments

The authors thank J. Casano and A. Miyaguchi for technical support, and A. Arkur and S. B. Shah for administrative assistance. The authors are grateful to the Weill Cornell Medical College Epigenomics Core Facility for next-generation sequencing (NGS) library preparation and sequencing for this study. The authors also thank the members of the Weill Cornell Flow Cytometry Core Facility and Sandra and Edward Meyer Cancer Center PDX shared resource.

This work was supported in part by the Italian Association for Cancer Research (AIRC, Milan, Italy), Metastases 5×1000 Special Program, and grant 21198 (R.F.); National Institutes of Health (NIH), National Cancer Institute (NCI) grants CA229086, CA229100, Leukemia and Lymphoma Society grant LLS 7011-16, departmental funds, and the Sandra and Edward Meyer Cancer Fund (G.I.); and the Rita-Levi Montalcini grant from the Italian Ministry of University and Research (MIUR) (D.F.). J.M.P. is supported by NIH NCI grant R01CA18710903S1. L.V.C. is supported by an American Italian Cancer Foundation (AICF) postdoctoral research fellowship. S.R. is funded by the Hartman Institute for Therapeutic Organ Regeneration; the Ansary Stem Cell Institute; NIH, National Heart, Lung, and Blood Institute grant R35 HL150809, NIH, National Institute of Diabetes and Digestive and Kidney Diseases grant RC2DK114777 and NIH, National Institute of Allergy and Infectious Diseases grant U01AI138329; the Empire State Stem Cell Board (C030160); the Daedalus Fund for Innovation; the Selma and Lawrence Ruben Science to Industry Bridge Fund from Weill Cornell Medicine; and the Starr Foundation stem cell core project and initiatives (TRI-SCI 2019-029).

Authorship

Contribution: L.V.C., D.F., J.M.P., L.Y., F.D.G., L. Cerchietti, S.R., and W.T. were responsible for conceptualization, formal analysis, methodology, writing-original draft, writing-review and editing; Y.H. and C.K. were responsible for formal analysis, methodology, and editing; W.C. was responsible for formal analysis and methodology; M.G., L. Consolino, and N.Z. were responsible for conceptualization, formal analysis, methodology, and editing; J.G.B.D. was responsible for conceptualization, methodology, and editing; F.B. was responsible for conceptualization, methodology, and editing; A.M.M., S.C., A.G., and R.F. were responsible for conceptualization, writing-review and editing; O.E. was responsible for conceptualization, formal analysis, writing-review and editing; and G.I. was responsible for conceptualization, data curation, formal analysis, supervision, methodology, writing-original draft, project administration, writing-review and editing.

Conflict-of-interest disclosure: M.G. is currently employed at Angiocrine Bioscience (San Diego, CA). S.R. is a cofounder and nonpaid consultant to Angiocrine Bioscience (San Diego, CA). The remaining authors declare no competing financial interests.

ORCID profiles: L.V.C., 0000-0001-8090-3880; D.F., 0000-0003-3004-6862; L.Y., 0000-0002-3040-8205; Y.H., 0000-0002-6348-874X; L. Consolino, 0000-0003-1667-4854; J.G.B.D., 0000-0003-4764-5503; N.Z., 0000-0002-9596-1095; A.M.M., 0000-0002-8074-2287; F.B., 0000-0003-1732-2033; L. Cerchietti, 0000-0003-0608-1350; G.I., 0000-0001-5566-0864.

Correspondence: Giorgio Inghirami, Department of Pathology and Laboratory Medicine, Weill Cornell Medicine, 1300 York Ave, New York, NY 10065; email: ggi9001@med.cornell.edu; Shahin Rafii, Hartman Institute for Therapeutic Organ Regeneration, Ansary Stem Cell Institute, Division of Regenerative Medicine, Department of Medicine, Weill Cornell Medicine, 1300 York Ave, New York, NY 10065; email: srafii@med.cornell.edu; and Leandro Cerchietti, Division of Hematology and Medical Oncology, Weill Cornell Medicine, 1300 York Ave, New York, NY 10065; email: lec2010@med.cornell.edu.

Footnotes

Submitted 11 January 2022; accepted 24 July 2022; prepublished online on *Blood* First Edition 18 August 2022. https://doi.org/10.1182/blood.2022015414.

*L.V.C., D.F., J.M.P., L.Y., and F.D.G. contributed equally to this work.

Presented as an oral abstract at the 63rd annual meeting of the American Society of Hematology, Atlanta, GA, December 2021. Abstract #704.

For original data, please contact corresponding author Giorgio Inhgirami at ggi9001@med.cornell.edu.

The online version of this article contains a data supplement.

There is a *Blood* Commentary on this article in this issue.

The publication costs of this article were defrayed in part by page charge payment. Therefore, and solely to indicate this fact, this article is hereby marked "advertisement" in accordance with 18 USC section 1734.

REFERENCES

1. Swerdlow SH, International Agency for Research on Cancer., Organization. WH. WHO classification of tumours of haematopoietic and lymphoid tissues. (ed Revised 4th). International Agency for Research on Cancer; 2017.
2. Bassan R, Hoelzer D. Modern therapy of acute lymphoblastic leukemia. *J Clin Oncol*. 2011;29(5):532-543.
3. Guru Murthy GS, Pondaiah SK, Abedin S, Atallah E. Incidence and survival of T-cell acute lymphoblastic leukemia in the United States. *Leuk Lymphoma*. 2019;60(5):1171-1178.
4. Pui CH, Robison LL, Look AT. Acute lymphoblastic leukaemia. *Lancet*. 2008;371(9617):1030-1043.
5. Conter V, Valsecchi MG, Buldini B, et al. Early T-cell precursor acute lymphoblastic leukaemia in children treated in AIEOP centres with AIEOP-BFM protocols: a retrospective analysis. *Lancet Haematol*. 2016;3(2):e80-86.
6. Pui CH, Pei D, Cheng C, et al. Treatment response and outcome of children with T-cell acute lymphoblastic leukemia expressing the gamma-delta T-cell receptor. *Oncoimmunology*. 2019;8(8):1599637.
7. Jain N, Lamb AV, O'Brien S, et al. Early T-cell precursor acute lymphoblastic leukemia/lymphoma (ETP-ALL/LBL) in adolescents and adults: a high-risk subtype. *Blood*. 2016;127(15):1863-1869.
8. Morita K, Jain N, Kantarjian H, et al. Outcome of T-cell acute lymphoblastic leukemia/lymphoma: Focus on near-ETP phenotype and differential impact of nelarabine. *Am J Hematol*. 2021;96(5):589-598.
9. Cullion K, Draheim KM, Hermance N, et al. Targeting the Notch1 and mTOR pathways in a mouse T-ALL model. *Blood*. 2009;113(24):6172-6181.
10. Maude SL, Dolai S, Delgado-Martin C, et al. Efficacy of JAK/STAT pathway inhibition in murine xenograft models of early T-cell precursor (ETP) acute lymphoblastic leukemia. *Blood*. 2015;125(11):1759-1767.
11. Chonghaile TN, Roderick JE, Glenfield C, et al. Maturation stage of T-cell acute lymphoblastic leukemia determines BCL-2 versus BCL-XL dependence and sensitivity to ABT-199. *Cancer Discov*. 2014;4(9):1074-1087.
12. Habets RA, de Bock CE, Serneels L, et al. Safe targeting of T cell acute lymphoblastic leukemia by pathology-specific NOTCH inhibition. *Sci Transl Med*. 2019;11(494):eaau624.
13. Delgado-Martin C, Meyer LK, Huang BJ, et al. JAK/STAT pathway inhibition overcomes IL7-induced glucocorticoid resistance in a subset of human T-cell acute lymphoblastic leukemias. *Leukemia*. 2017;31(12):2568-2576.
14. Zhang J, Ding L, Holmfeldt L, et al. The genetic basis of early T-cell precursor acute lymphoblastic leukaemia. *Nature*. 2012;481(7380):157-163.
15. Ayala F, Dewar R, Kieran M, Kalluri R. Contribution of bone microenvironment to leukemogenesis and leukemia progression. *Leukemia*. 2009;23(12):2233-2241.
16. Passaro D, Quang CT, Ghysdael J. Microenvironmental cues for T-cell acute lymphoblastic leukemia development. *Immunol Rev*. 2016;271(1):156-172.
17. Pitt LA, Tikhonova AN, Hu H, et al. CXCL12-producing vascular endothelial niches control acute T cell leukemia maintenance. *Cancer Cell*. 2015;27(6):755-768.
18. Passaro D, Irigoyen M, Catherinet C, et al. CXCR4 is required for leukemia-initiating cell activity in T cell acute lymphoblastic leukemia. *Cancer Cell*. 2015;27(6):769-779.
19. Duan CW, Shi J, Chen J, et al. Leukemia propagating cells rebuild an evolving niche in response to therapy. *Cancer Cell*. 2014;25(6):778-793.
20. Butler JM, Kobayashi H, Rafii S. Instructive role of the vascular niche in promoting tumour growth and tissue repair by angiocrine factors. *Nat Rev Cancer*. 2010;10(2):138-146.
21. Nagl L, Horvath L, Pircher A, Wolf D. Tumor endothelial cells (tecs) as potential immune directors of the tumor microenvironment - new findings and future perspectives. *Front Cell Dev Biol*. 2020;19(8):766.
22. Jiang Y, Guo Y, Hao J, et al. Development of an arteriolar niche and self-renewal of breast cancer stem cells by lysophosphatidic acid/protein kinase D signaling. *Commun Biol*. 2021;4(1):780.
23. Vadillo E, Dorantes-Acosta E, Pelayo R, Schnoor M. T cell acute lymphoblastic leukemia (T-ALL): New insights into the cellular origins and infiltration mechanisms common and unique among hematologic malignancies. *Blood Rev*. 2018;32(1):36-51.
24. Sipkins DA, Wei X, Wu JW, et al. In vivo imaging of specialized bone marrow endothelial microdomains for tumour engraftment. *Nature*. 2005;435(7044):969-973.
25. Cao Z, Scandura JM, Inghirami GG, Shido K, Ding BS, Rafii S. Molecular checkpoint decisions made by subverted vascular niche transform indolent tumor cells into chemoresistant cancer stem cells. *Cancer Cell*. 2017;31(1):110-126.
26. McMillin DW, Negri JM, Mitsiades CS. The role of tumour-stromal interactions in modifying drug response: challenges and opportunities. *Nat Rev Drug Discov*. 2013;12(3):217-228.
27. Bakker E, Qattan M, Mutti L, Demonacos C, Krstic-Demonacos M. The role of microenvironment and immunity in drug response in leukemia. *Biochim Biophys Acta*. 2016;1863(3):414-426.
28. Habiel DM, Krepostman N, Lilly M, et al. Senescent stromal cell-induced divergence and therapeutic resistance in T cell acute lymphoblastic leukemia/lymphoma. *Oncotarget*. 2016;7(50):83514-83529.
29. Fahy L, Calvo J, Chabi S, et al. Hypoxia favors chemoresistance in T-ALL through an HIF1alpha-mediated mTORC1 inhibition loop. *Blood Adv*. 2021;5(2):513-526.
30. Hopken UE, Rehm A. Targeting the tumor microenvironment of leukemia and lymphoma. *Trends Cancer*. 2019;5(6):351-364.
31. Sharma P, Hu-Lieskovan S, Wargo JA, Ribas A. Primary, adaptive, and acquired resistance to cancer immunotherapy. *Cell*. 2017;168(4):707-723.
32. Seandel M, Butler JM, Kobayashi H, et al. Generation of a functional and durable vascular niche by the adenoviral E4ORF1 gene. *Proc Natl Acad Sci U S A*. 2008;105(49):19288-19293.
33. Cao Z, Ding BS, Guo P, et al. Angiocrine factors deployed by tumor vascular niche induce B cell lymphoma invasiveness and chemoresistance. *Cancer Cell*. 2014;25(3):350-365.
34. Townsend EC, Murakami MA, Christodoulou A, et al. The Public Repository of Xenografts enables discovery and randomized phase II-like trials in mice. *Cancer Cell*. 2016;29(4):574-586.
35. Qin H, Dong Z, Wang X, et al. CAR T cells targeting BAFF-R can overcome CD19

antigen loss in B cell malignancies. *Sci Transl Med*. 2019;11(511):eaaw9414.

36. Butler JM, Nolan DJ, Vertes EL, et al. Endothelial cells are essential for the self-renewal and repopulation of Notch-dependent hematopoietic stem cells. *Cell Stem Cell*. 2010;6(3):251-264.

37. Kobayashi H, Butler JM, O'Donnell R, et al. Angiocrine factors from Akt-activated endothelial cells balance self-renewal and differentiation of haematopoietic stem cells. *Nat Cell Biol*. 2010;12(11):1046-1056.

38. Laranjeira AB, de Vasconcellos JF, Sodek L, et al. IGFBP7 participates in the reciprocal interaction between acute lymphoblastic leukemia and BM stromal cells and in leukemia resistance to asparaginase. *Leukemia*. 2012;26(5):1001-1011.

39. Markovic A, MacKenzie KL, Lock RB. Induction of vascular endothelial growth factor secretion by childhood acute lymphoblastic leukemia cells via the FLT-3 signaling pathway. *Mol Cancer Ther*. 2012;11(1):183-193.

40. Teschendorff AE, Enver T. Single-cell entropy for accurate estimation of differentiation potency from a cell's transcriptome. *Nat Commun*. 2017;8:15599.

41. Lezon TR, Banavar JR, Cieplak M, Maritan A, Fedoroff NV. Using the principle of entropy maximization to infer genetic interaction networks from gene expression patterns. *Proc Natl Acad Sci U S A*. 2006;103(50):19033-19038.

42. Aifantis I, Raetz E, Buonamici S. Molecular pathogenesis of T-cell leukaemia and lymphoma. *Nat Rev Immunol*. 2008;8(5):380-390.

43. Van Vlierberghe P, Ferrando A. The molecular basis of T cell acute lymphoblastic leukemia. *J Clin Invest*. 2012;122(10):3398-3406.

44. Chen B, Tan Z, Gao J, et al. Hyperphosphorylation of ribosomal protein S6 predicts unfavorable clinical survival in non-small cell lung cancer. *J Exp Clin Cancer Res*. 2015;34:126.

45. Pallis M, Harvey T, Russell N. Phenotypically dormant and immature leukaemia cells display increased ribosomal protein S6 phosphorylation. *PLoS One*. 2016;11(3):e0151480.

46. Vlachos A. Acquired ribosomopathies in leukemia and solid tumors. *Hematology Am Soc Hematol Educ Program*. 2017;2017(1):716-719.

47. Zhang P, Lu Y, Gao S. High-mobility group box 2 promoted proliferation of cervical cancer cells by activating AKT signaling pathway. *J Cell Biochem*. 2019;120(10):17345-17353.

48. Kwon JH, Kim J, Park JY, et al. Overexpression of high-mobility group box 2 is associated with tumor aggressiveness and prognosis of hepatocellular carcinoma. *Clin Cancer Res*. 2010;16(22):5511-5521.

49. Qiu JJ, Lin XJ, Tang XY, Zheng TT, Lin YY, Hua KQ. Exosomal metastasis associated lung adenocarcinoma transcript 1 promotes angiogenesis and predicts poor prognosis in epithelial ovarian cancer. *Int J Biol Sci*. 2018;14(14):1960-1973.

50. Gu Y, Jasti AC, Jansen M, Siefring JE. RhoH, a hematopoietic-specific Rho GTPase, regulates proliferation, survival, migration, and engraftment of hematopoietic progenitor cells. *Blood*. 2005;105(4):1467-1475.

51. Park JE, Botting RA, Dominguez Conde C, et al. A cell atlas of human thymic development defines T cell repertoire formation. *Science*. 2020;367(6480):eaay3224.

52. Le J, Park JE, Ha VL, et al. Single-cell RNA-Seq mapping of human thymopoiesis reveals lineage specification trajectories and a commitment spectrum in T cell development. *Immunity*. 2020;52(6):1105-1118.e1109.

53. D'Souza B, Meloty-Kapella L, Weinmaster G. Canonical and non-canonical Notch ligands. *Curr Top Dev Biol*. 2010;92:73-129.

54. Pietras A, von Stedingk K, Lindgren D, Pahlman S, Axelson H. JAG2 induction in hypoxic tumor cells alters Notch signaling and enhances endothelial cell tube formation. *Mol Cancer Res*. 2011;9(5):626-636.

55. Tamura K, Hashimoto K, Suzuki K, Yoshie M, Kutsukake M, Sakurai T. Insulin-like growth factor binding protein-7 (IGFBP7) blocks vascular endothelial cell growth factor (VEGF)-induced angiogenesis in human vascular endothelial cells. *Eur J Pharmacol*. 2009;610(1-3):61-67.

56. Cheng SM, Chang YC, Liu CY, et al. YM155 down-regulates survivin and XIAP, modulates autophagy and induces autophagy-dependent DNA damage in breast cancer cells. *Br J Pharmacol*. 2015;172(1):214-234.

57. Dai Y, Chen S, Pei XY, et al. Interruption of the Ras/MEK/ERK signaling cascade enhances Chk1 inhibitor-induced DNA damage in vitro and in vivo in human multiple myeloma cells. *Blood*. 2008;112(6):2439-2449.

58. Zong CS, Chan J, Levy DE, Horvath C, Sadowski HB, Wang LH. Mechanism of STAT3 activation by insulin-like growth factor I receptor. *J Biol Chem*. 2000;275(20):15099-15105.

59. Waibel M, Vervoort SJ, Kong IY, et al. Epigenetic targeting of Notch1-driven transcription using the HDACi panobinostat is a potential therapy against T-cell acute lymphoblastic leukemia. *Leukemia*. 2018;32(1):237-241.

60. Bride KL, Vincent TL, Im SY, et al. Preclinical efficacy of daratumumab in T-cell acute lymphoblastic leukemia. *Blood*. 2018;131(9):995-999.

61. Mshaik R, Simonet J, Georgievski A, et al. HSP90 inhibitor NVP-BEP800 affects stability of SRC kinases and growth of T-cell and B-cell acute lymphoblastic leukemias. *Blood Cancer J*. 2021;11(3):61.

62. Verbeke D, Gielen O, Jacobs K, et al. Ruxolitinib synergizes with dexamethasone for the treatment of T-cell acute lymphoblastic leukemia. *Hemasphere*. 2019;3(6):e310.

63. Frismantas V, Dobay MP, Rinaldi A, et al. Ex vivo drug response profiling detects recurrent sensitivity patterns in drug-resistant acute lymphoblastic leukemia. *Blood*. 2017;129(11):e26-e37.

64. Shi WY, Wang L, Xiao D, et al. Proteasome inhibitor bortezomib targeted tumor-endothelial cell interaction in T-cell leukemia/lymphoma. *Ann Hematol*. 2011;90(1):53-58.

65. Indraccolo S, Minuzzo S, Masiero M, et al. Cross-talk between tumor and endothelial cells involving the Notch3-Dll4 interaction marks escape from tumor dormancy. *Cancer Res*. 2009;69(4):1314-1323.

66. Spiegel A, Kollet O, Peled A, et al. Unique SDF-1-induced activation of human precursor-B ALL cells as a result of altered CXCR4 expression and signaling. *Blood*. 2004;103(8):2900-2907.

67. Teicher BA, Fricker SP. CXCL12 (SDF-1)/CXCR4 pathway in cancer. *Clin Cancer Res*. 2010;16(11):2927-2931.

68. Schwartzman O, Savino AM, Gombert M, et al. Suppressors and activators of JAK-STAT signaling at diagnosis and relapse of acute lymphoblastic leukemia in Down syndrome. *Proc Natl Acad Sci U S A*. 2017;114(20):E4030-E4039.